

Development of 1 kW class polymer electrolyte membrane fuel cell power generation system

H.I. Lee^{*}, C.H. Lee, T.Y. Oh, S.G. Choi, I.W. Park, K.K. Baek

Hyundai Industrial Research Institute, Hyundai Heavy Industries Co. Ltd., 1 Cheonha-Dong, Dong-Gu, Ulsan, South Korea

Received 18 July 2001; accepted 31 October 2001

Abstract

Regarding the reliability of the polymer electrolyte membrane (PEM) fuel cell, the advancement of fuel, thermal and water management techniques of the system have been critically investigated. In this study, a 1 kW class PEM fuel cell stack is built with an Aciplex-STM membrane, which is integrated to be automatically controlled in a hydrogen-fueled power generation system of a 80 cm × 70 cm × 120 cm single unit with a dc/ac inverter which produces 220 VAC power. Intensive and systematic care should be taken especially with the longer cell stack which is being operated under repeated current load change. The automatically controlled fuel-feed and thermal management system achieved in this study can markedly enhance the fuel efficiency and the reliability of the cell stack. The devices in the sub-systems are all electrically controlled versions to be manipulated on a touch screen via a PLC unit. The thermal and fuel-feed control logic are pre-built-in the CPU of the PLC unit based on an early study of cell stack evaluation. In addition, the power inverting and dummy load unit is coupled to the power generation system, and an additional data acquisition system has been constructed. © 2002 Elsevier Science B.V. All rights reserved.

Keywords: Polymer electrolyte membrane fuel cell; Power generation system; Reliability; Fuel management; Thermal management; Water management

1. Introduction

It is anticipated that full-fledged commercialization of fuel cells by a few promising major suppliers will be realized early in new millennium. The fuel cell commercial products in the 21st century will be for vehicular engines, power sources for electronic devices, or residential power modules all of which will be equipped with the polymer electrolyte membrane (PEM) fuel cell. For their successful introduction, however, there are critical issues to be challenged, such as reliability for long-term service life, cost-reduction of their components, and a nation- or world-wide fuel distribution and supply strategy. On the other hand, the application of PEM fuel cells in the heavy industrial sector has been barely attempted compared with those of solid oxide fuel cell (SOFC), molten carbonate fuel cell (MCFC) and phosphoric acid fuel cell (PAFC) systems. Early trials of PEM fuel cell power generation systems in submarines in Germany and Canada recently released were encouraging events [1]. The systems would, however, be neither expected to be commercially viable nor be widely applicable to other applications. As a matter of fact, the demand for the commercialization of large scale fuel cell products in heavy

industries is far less urgent than that for automotive industries. The 10% production quota of zero-emission vehicle (ZEV) in California, USA, currently due in 2003, has drawn strong interest as well as huge investment from auto-makers to develop PEM fuel cell technology. It is no more far-fetched to say that such a world-wide environmental regulation and social industrial demand will be intensified and extended to other industrial sectors.

Based on previous studies by the authors with a mono-cell and a smaller scale stack, a prototype power generation system with a middle stack of the 1 kW class has been developed as an intermediary step in the ultimate goal of a 2 kW PEM fuel cell power module [2–4]. In a preliminary study, all variables for a membrane and electrode assembly (MEA) along with the parameters for their operation were evaluated to optimize these parameters in terms of the electrical performance. In a study of the middle stack of the 1 kW class, the primary focus was clarification of the deterioration mechanism of the cell stack and the development of the most effective measure to prevent it. The automatic control logic for the 1 kW PEM fuel power generation system was designed based on previous studies. The developed power generation system was designed in terms of control schemes for the gas feed to the cell stack and its thermal condition so as to tune it to the change in the external load. Ongoing efforts will be directed to the

^{*} Corresponding author. Tel.: +82-52-230-5513; fax: +82-52-230-3445.
E-mail address: hilee@hhi.co.kr (H.I. Lee).

realization of more compact and user-friendly modules of the 2 kW class for industrial or home power sources. These experience in small-scale PEM fuel cell power generation systems are a useful basis to meet the expected future demand for large-scale fuel cell power generation systems for heavy industrial use.

2. Experimental and results

2.1. Mono-cell

A single MEA was made by interposing a piece of perfluorosulfonic acid membrane between two catalyzed carbon electrodes of E-tek[®], which had been pre-impregnated with electrolyte solution on their catalyzed front surfaces. The prepared assembly was hot-pressed at 135 °C at 1–3 metric ton. The electrical performance of each MEA was evaluated with a model GT-500, Globetech[®] fuel cell test station which consisted of a gas feed and load unit with a GPIB[™]-interfaced PC.

The membrane was pre-treated in H₂O₂ solution to remove organic matter, followed by treatment in sulfuric acid to promote ionic conductivity by substituting $-\text{Na}^+$ with $-\text{H}^+$. No variables of the membrane treatment procedure were evaluated for MEAs electrical performance. Electrolytic membranes from DuPont[®] and Asahi Chemicals[®] were separately used in mono-cell fabrication.

The Nafion-115[™] membrane was chosen as the best material for study on the basis of its physical strength and ionic conductivity. The Aciplex-S[™] membrane of Asahi Chemicals[®], which is not yet commercially available, was found to be better in terms of chemical and physical properties. Thus, it was used for the middle stack of 1 kW class. Being equal in all other conditions, the electrical performance of MEA with Aciplex-S[™] was better than that with Nafion-115[™], as shown in Fig. 1. It was inferred that higher equivalent weight of Aciplex-S[™] gave higher proton conductivity and resulted in higher electrical performance.

The front surface of the electrode was pre-impregnated with the same grade of electrolytic solution that was used to prepare the MEA in order to utilize fully its effective area of the three-phase interface. Many other researchers have studied how to apply the electrolytic solution to the electrode more effectively, as the brushing method, used in this study, is far less time-effective with low reproducibility [5,6]. As far as the brushing method is concerned a 0.6 mg/cm² loading of electrolytic solution was found to be the most effective, assuming that a standardized brushing procedure is used. It is shown in Fig. 2 that the greater the loading amount beyond 0.6 mg/cm², the poorer is the electrical performance of the MEA.

The amount of factory-loaded Pt catalyst on the front surface of the electrode is one of the primary factors that determine the electrical performance of MEA. As seen in

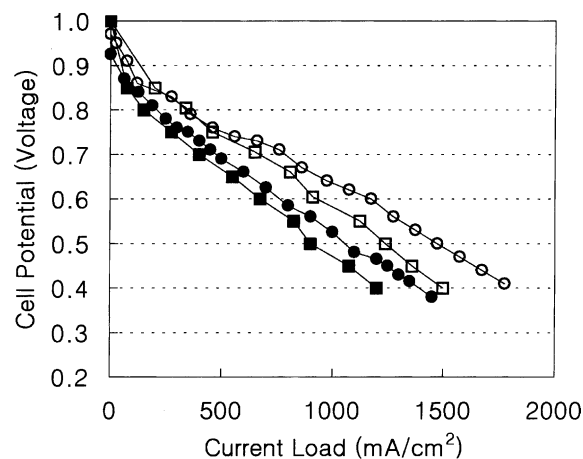


Fig. 1. Electrical performance curves of MEAs with Nafion-115[™] and Aciplex-S[™] membrane, 70 °C cell temperature, hydrogen-fueled condition: (■) Nafion[™]-115 (1 atm); (□) Nafion[™]-115 (3 atm); (●) Aciplex[™] (1 atm); (○) Aciplex[™] (3 atm).

Fig. 3, the MEA with 2 mg/cm² Pt-loaded electrodes shows a less steep slope of the *I*-*V* curve. On the other hand, MEAs with 1 and 0.4 mg/cm² Pt-loaded electrodes have a barely discernible difference in the slopes of their *I*-*V* curves, especially in the high current region. The improvement of catalyst substrate structure or its fabrication process is considered to be a critical step to reduce the effective amount of loaded catalyst [7–9]. In addition to the factors addressed above, the effects of cell temperature, operation pressure, and reactant gas flow rate on the cell stack performance were also evaluated to provide a basis for ongoing studies on cell stacks.

2.2. Short stack

The technological issues arising from cell stacking was studied by using short stacks of 100 and 200 W capacity. The stacks consisted, respectively, of 5 and 10 cells of

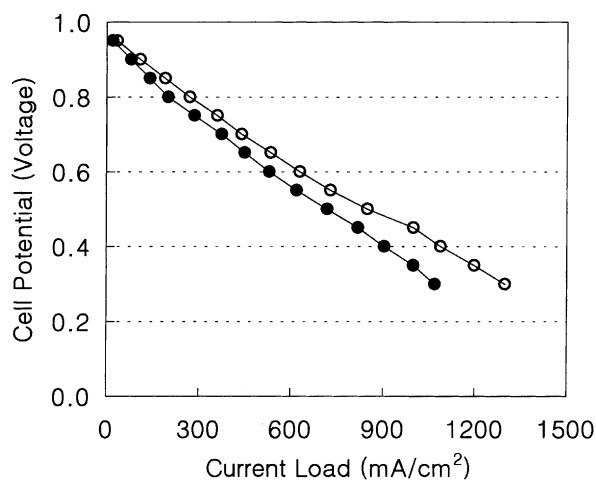


Fig. 2. Electrical performance curves of MEAs with electrolytic loading, 40 °C cell temperature, hydrogen-fueled and atmospheric pressure conditions: (○) 0.6 mg/cm²; (●) 1.0 mg/cm².

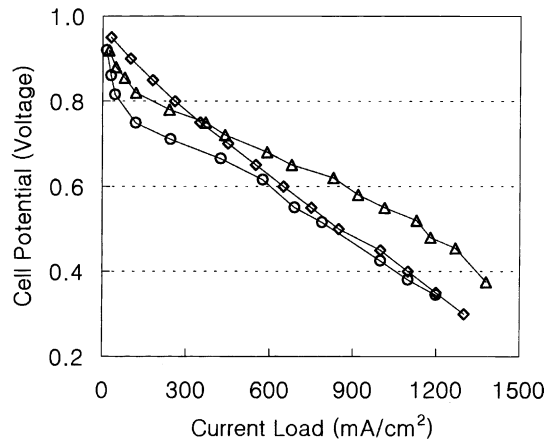


Fig. 3. Electrical performance curves of MEAs with catalyst loading, 70 °C cell temperature, hydrogen-fueled and atmospheric pressure condition: (○) 0.4 mg/cm² Pt; (◇) 1.0 mg/cm² Pt; (△) 2.0 mg/cm² Pt.

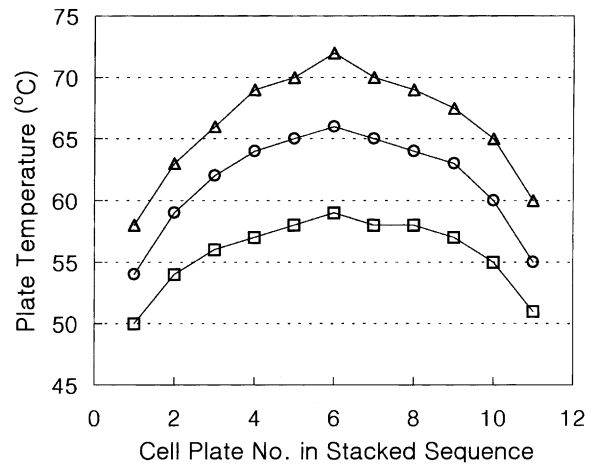


Fig. 5. Heat generation behavior of 10-cell stack at 300 mA/cm² current load with elapse of time without additional heating and cooling: (□) 5 min; (○) 10 min; (△) 20 min.

Nafion-115TM-based MEA with 50 cm² active area and were designed to incorporate an additional water cooling plate and to be externally humidified. First of all, the thermal condition over the cell stack was evaluated to determine the critical current load before cooling is required. The representative temperature of five-cell stack of 100 W capacity measured at the metal tie end-plate was expected to overshoot the designed temperature of 70 °C at 600 mA/cm² as shown in Fig. 4. Below 600 mA/cm², the temperature curves with time gave a plateau at a lower temperature than the designed value. Thus, there was no need for additional cooling. With increase in stacked cell number, more concern for thermal disparity along the stack length arises. Thus, for

a 10-cell stack of 200 W capacity, the temperature of each cell plate was monitored with a K-type thermocouple which was implanted in the cell plate. The temperature was recorded after the tie end-plate temperature reached a pre-determined value of 50 °C. The data in Fig. 5 show that the critical maximum current load was 300 mA/cm² for a 10-cell stack to prevent overheating above the designed temperature of 70 °C in the mid cell. To optimize the cooling conditions under higher loads, two additional cooling plates were inserted into the mid-section of the cell stack. By controlling the water pump, the coolant water feed rate was regulated to maintain the stack temperature within a design scheme. With such a control scheme the thermal condition of

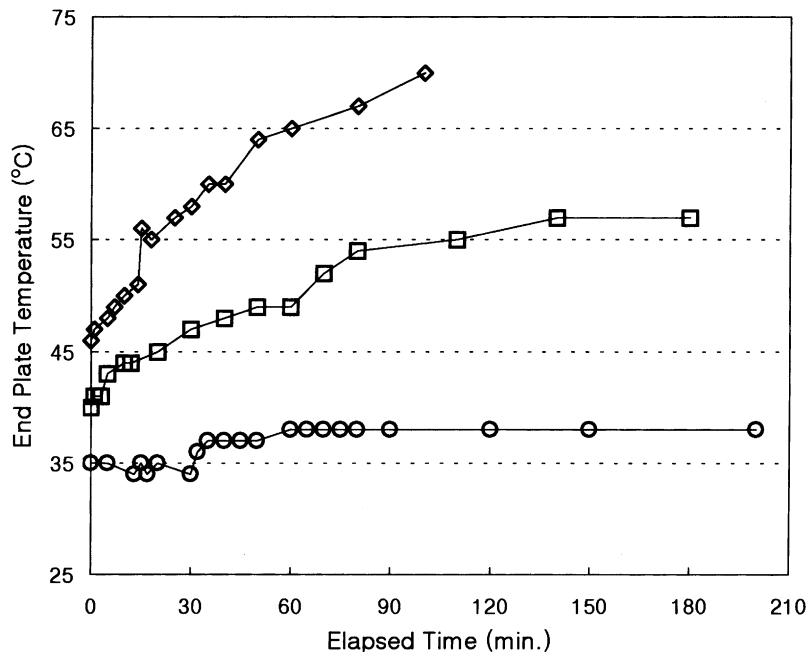


Fig. 4. Heat generation behaviors of five-cell stack with elapse of operation time without additional heating and cooling: (○) 200 mA/cm²; (□) 400 mA/cm²; (◇) 600 mA/cm².

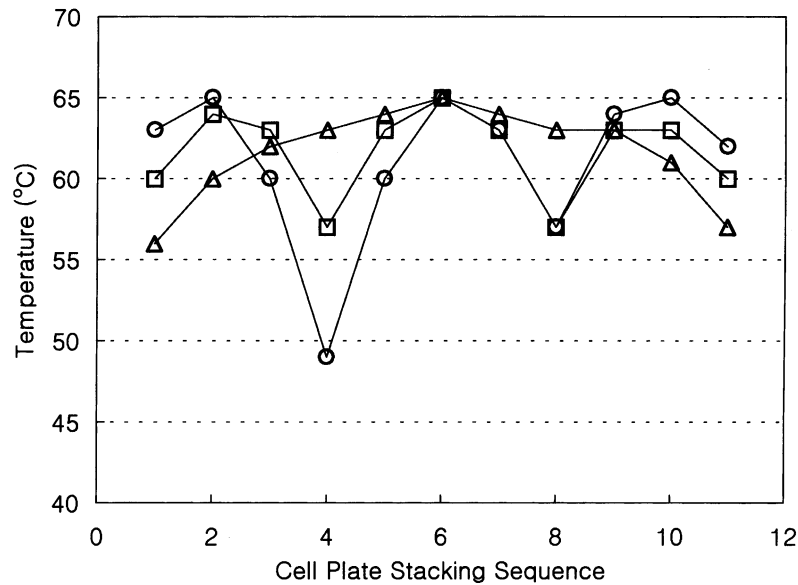


Fig. 6. Optimized cell stack temperature distribution over 10-cell stack with proper cooling measure and control with variation of current load: (Δ) 200 mA/cm²; (\square) 400 mA/cm²; (\circ) 600 mA/cm².

the 10-cell stack could be optimized with current load change (see Figs. 6 and 7).

On the other hand, the fuel supply strategy should also be re-established for a multiple cell stack. In a mono-cell, the optimum fuel rate is known to be $1.3 \times$ stoichiometry. With a fuel-feed rate below $1.0 \times$ stoichiometry, so-called fuel depletion will occur at some local region in the MEA and result in irreversible deterioration of the MEA. This behavior has been widely recognized by other workers. At feed rates over $1.0 \times$ stoichiometry, it is not until the rate reaches $10 \times$ stoichiometry that the cell potential took a steep downturn to a nearly under-limit potential as shown in Fig. 8. This is attributed to facilitation of the dry-out of the MEA and reduction of the fuel gas diffusion efficiency to the MEA by extremely high fuel gas feed rate.

In case of multicell stacks early trials of fuel-feed with theoretical equation, i.e. $n(\text{stacked cell number}) \times (1.3 \times \text{stoichiometry})$, revealed a cell potential drop in the negative direction in the MEAs (at the end side of fuel inlet of the stack) so that the fuel-feed rate for the multicell stack must be set at a quite high end. The optimum fuel-feed rate with current load change is shown in Fig. 9. It is seen that, in the lower load range, higher fuel-feed rates are necessary. This value should be established for each of the multicell stacks, case by case.

2.3. Middle stack and deterioration mechanism by fuel depletion

On the basis of an earlier study, the middle stack of the 1 kW class was built with the design scheme given in Table 1.

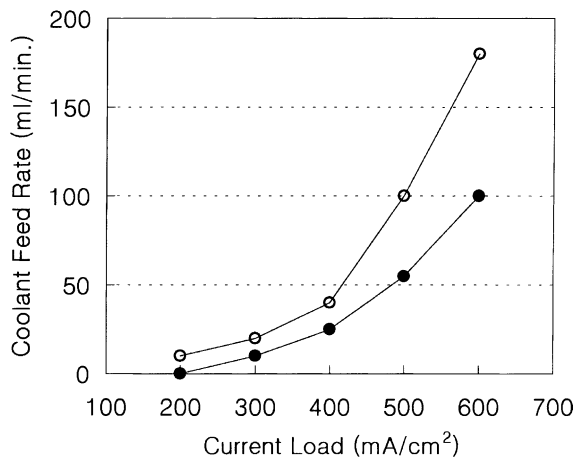


Fig. 7. Proper coolant feed rate for optimized temperature distribution over 10-cell stack with variation of current load: (\circ) 60 °C stack temperature; (\bullet) 65 °C stack temperature.

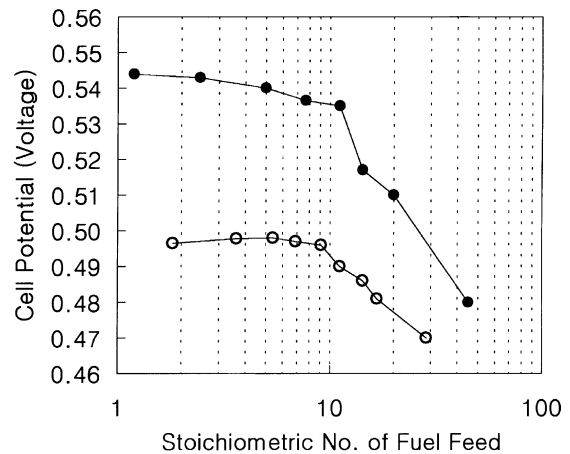


Fig. 8. Cell potential and fuel-feed rate relationship in mono-cell: (\bullet) 400 mA/cm²; (\circ) 600 mA/cm².

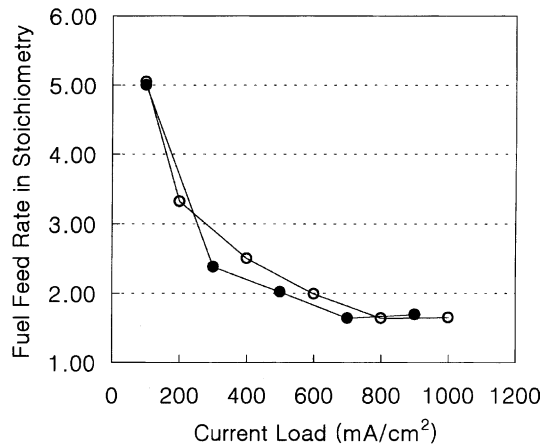


Fig. 9. Optimum fuel-feed rate in short stacks with current load variation to achieve stable cell stack performance without fuel starvation: (●) four-cell stack; (○) 10-cell stack.

Table 1
Design specification of 1 kW class stack

Item	Specification
Cell no. to be stacked	30 cells
Active electrode area	50 cm ²
Stack dimensions	20 cm × 20 cm × 50 cm
Electrolytic membrane	Aciplex-S TM
Current load range	0~50 A
Stack voltage range	15~30 V
Nominal current load	30 ± 5 A
Nominal stack voltage	20 ± 2 V
Nominal electrical output	700 W
Maximum electrical output	1000 W
Fuel/oxidant	Pure hydrogen/pure oxygen

Fuel and oxidant gases are passed through an internal humidification section and then the humidified gases are fed to each cell in a parallel mode. Liquid water travels across cooling plates allocated at every three cells, and then

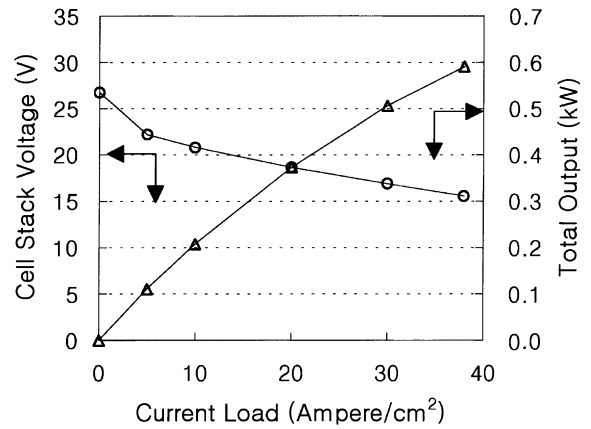


Fig. 10. Rated output curve of 29-cell stack with cell stack voltage curves with current load: (○) cell stack voltage; (△) total electrical output.

is used to humidify the reactant gases in the humidification section. The first trial of the electrical power rating, gave around 600 W, as shown in Fig. 10. This poor performance is explained by the data given in Fig. 11. The cell voltage in the far end of the stack (i.e. away from the fuel inlet) is found to plummet with increase in current load. Previous studies in short stacks could not fully cover the critical issue of improper fuel-feed in a far longer stack. It is not easy to predict the optimum fuel-feed strategy for each different stack, until the overall stack design is developed to a standard pattern.

To clarify the cell deterioration mechanism by mal-management of fuel-feed, a further study was conducted. The damaged cell of the stack was removed for surface observation. This revealed that not only the cell material but also the front surface of the bipolar plate had suffered damage. There was a pinhole in the membrane sheet as well as numerous corrosion pits with a sticky debris of the carbon cloth of the electrode on the front surface of the fuel side of the bipolar plate. It is assumed that the fuel depletion in the active

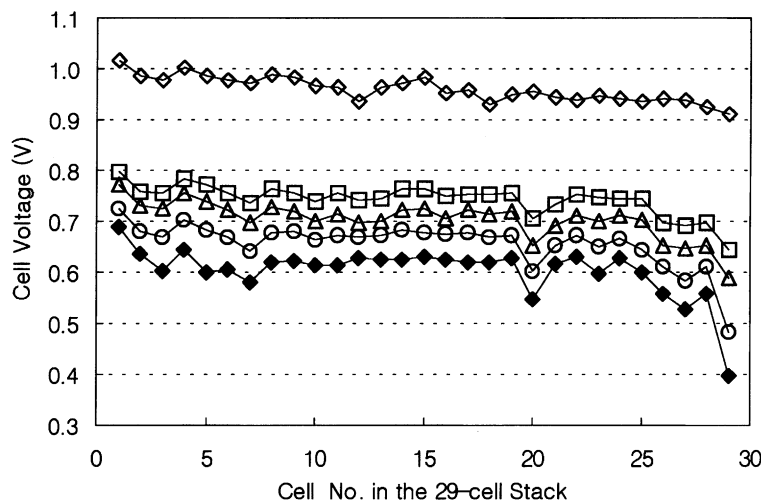


Fig. 11. Cell voltage distribution over 29-cell stack with variation of current load, 70 °C average cell stack temperature, hydrogen-fueled, atmospheric pressure conditions: (◇) open-circuit potential; (□) 6 A; (△) 10 A; (○) 18 A; (◆) 30 A.

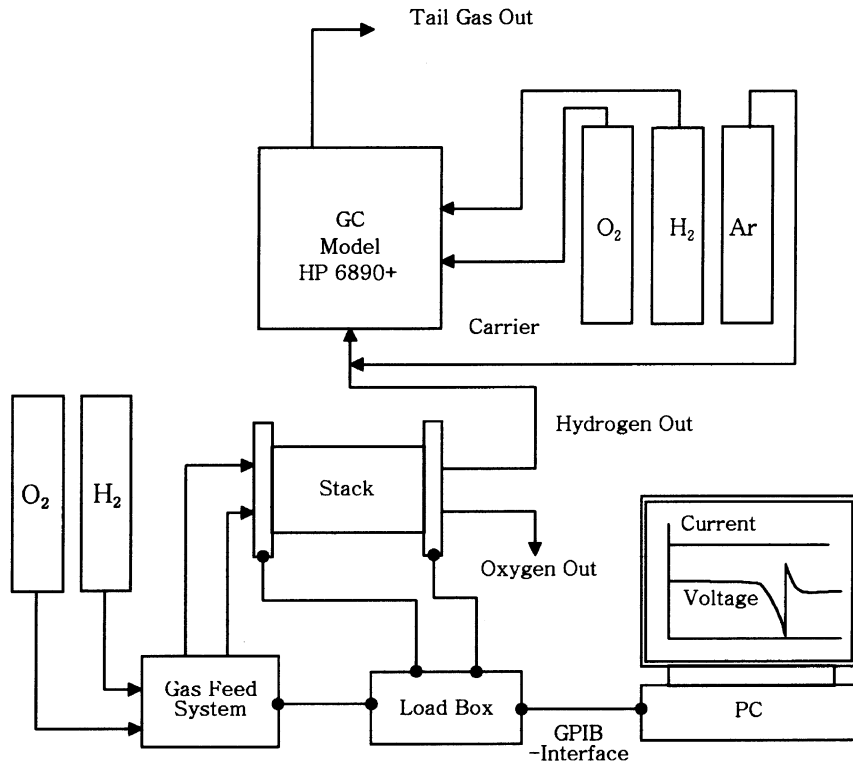
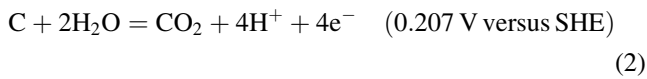
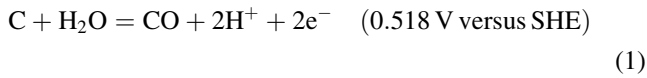


Fig. 12. Schematic diagram of gas chromatographic (GC) analysis system.

electrode surface facilitates flooding and corrosion of cell components. The liquid water and carbon element in the cell component react as follows:



The above two reactions were proposed for a PAFC by Mitsuda and Murahashi [10]. To confirm these reactions in a PEM fuel cell, gas chromatographic (GC) analysis was conducted with the analysis system shown in Fig. 12, during an artificial fuel depletion condition with a flame ionization detector (FID) and a thermal conductivity detector (TCD). The exhaust gas from the cell was balanced with argon gas in all analysis test. Prior to the main analysis, a qualitative and quantitative basis for the specific gas species was established. The qualitative results are listed in Table 2. From GC analysis curves, each gas species can be identifiable by their specific retention time. All six kinds of standard mixed gases of H₂, O₂, CO, and CO₂ were tested on a quantitative base, of which four test results for the high-end of CO and CO₂ content are presented in Fig. 13. The CO and CO₂ contents in the standard mixed gases were prepared to cover the ranges (1.15 ppm–1.03%) and (1.99 ppm–30%) for CO and CO₂, respectively. From these results, quantitative equations for each gas species were derived as Eqs. (3)–(7). An area of an

analysis curve could be converted to the contents of each gas species in the exhaust gas from the cell stack with

$$Y(H_2\text{-TCD area}) = 2.791 \times 10^6 + 1.937 \times 10^7 (H_2, \%) \quad (3)$$

$$Y(O_2\text{-TCD area}) = -1.554 \times 10^5 + 3.714 \times 10^6 (O_2, \%) \quad (4)$$

$$Y(CO_2\text{-TCD area}) = 2.681 \times 10^5 + 1.973 \times 10^6 (CO_2, \%) \quad (5)$$

$$Y(CO_2\text{-FID area}) = -2.992 \times 10^5 + 1.004 \times 10^7 (CO, \text{ppm}) \quad (6)$$

$$Y(CO_2\text{-FID area}) = -3.096 \times 10^8 + 9.683 \times 10^8 (CO_2, \%) \quad (7)$$

Table 2
Qualitative GC analysis

Species	TCD analysis		Species	FID analysis	
	Retention time (min)	Comment		Retention time (min)	Comment
H ₂	0.78	–	CO	0.95	–
O ₂	0.91	Peak overlap	CO ₂	1.77	–
CO	0.91	Peak overlap	–	–	–
CO ₂	1.70	–	–	–	–

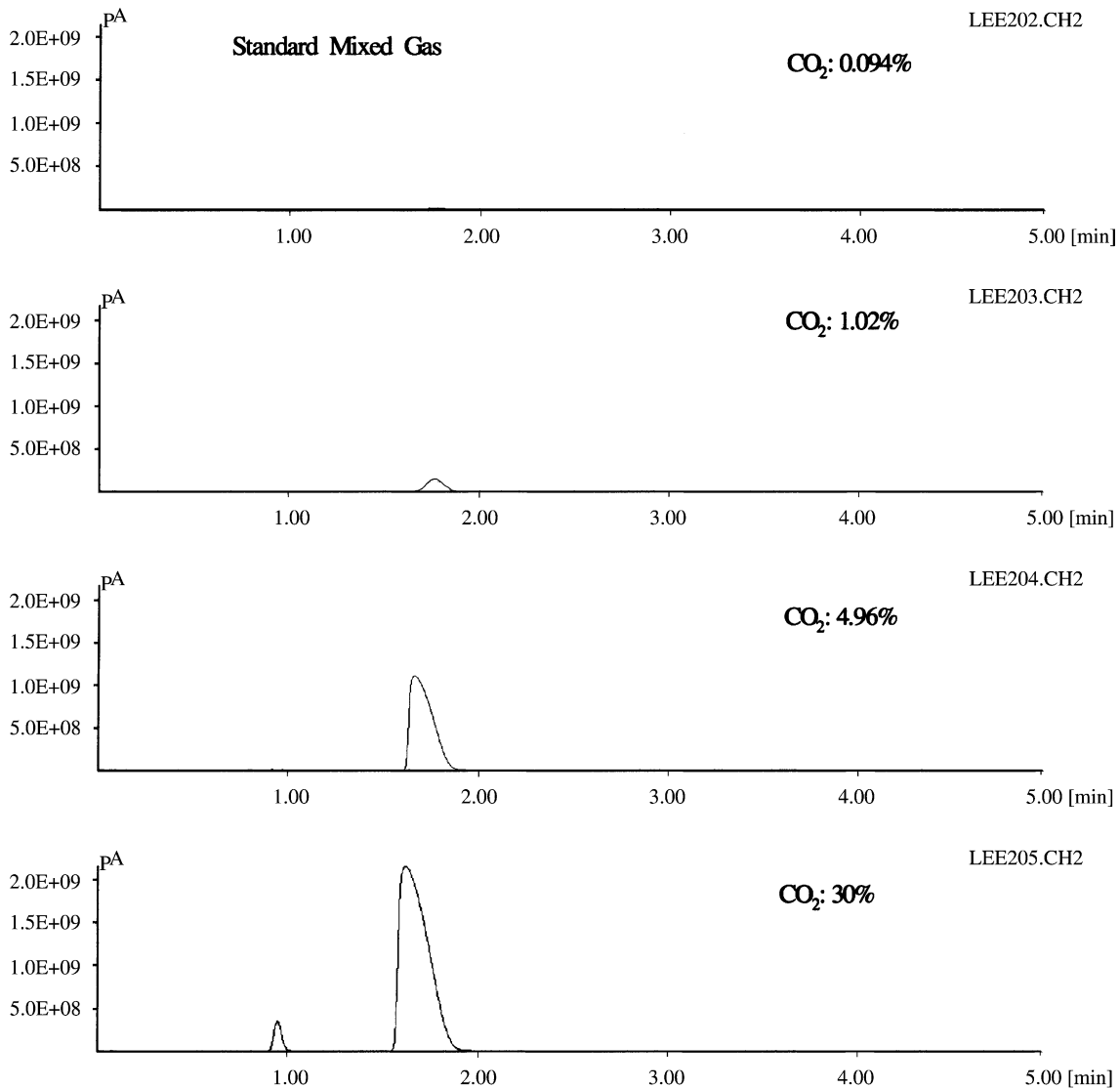


Fig. 13. GC analysis results of standard mixed gases for quantitative basis.

In the main test, the fuel depletion condition was artificially simulated by the abrupt reduction of fuel-feed rate down to $0.8 \times$ stoichiometry during operation with a normal feed rate ($1.3 \times$ stoichiometry) as shown in Fig. 14. The fuel-feed was forced to recover the normal condition before the cell voltage plummet to the negative direction. A small sample of the exhaust gas was extracted just before the cell voltage up-turn to positive direction. The test result for the fuel depletion condition revealed that fuel starvation could induce a sharp rise in CO and CO₂ generation (see Fig. 15). This indicates the corrosion of carbon material. Besides causing corrosion damage, CO is a harmful species to catalyst and the damage would be irreparable if the cell remained in this condition for an extend duration. Thus, to secure the high reliability and long-term service life of a cell stack, extreme care should be taken to prevent local or whole fuel depletion.

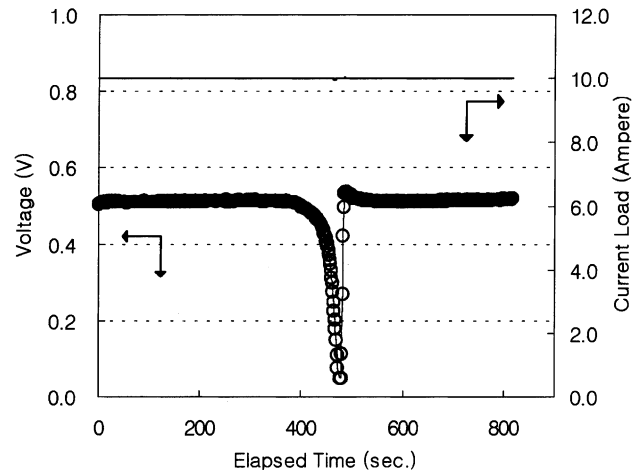


Fig. 14. Artificially simulated condition for fuel depletion conditions: (○) current load; (—) cell voltage.

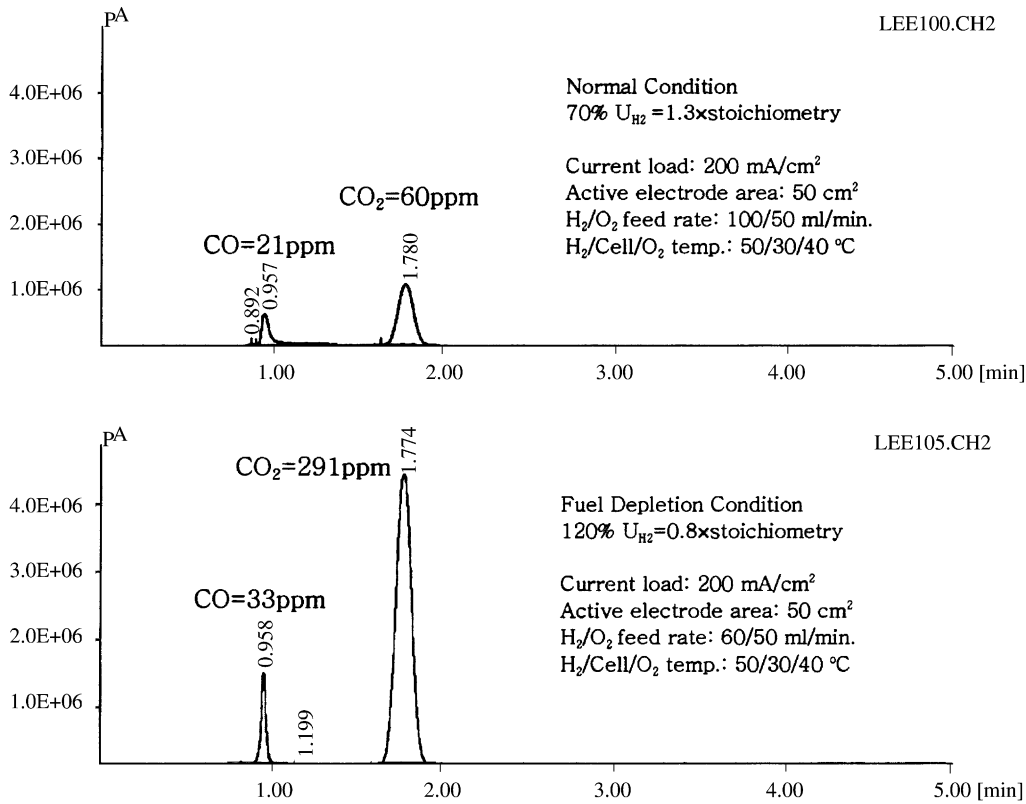


Fig. 15. GC analysis (FID) curves for normal and fuel depletion condition.

2.4. Power generation system

The power generation system consisted of three major parts namely: power generation unit, control unit, and inverting and dummy load unit. The 1 kW class cell stack, fuel and oxidant gas management sub-system, cooling sub-system, and heat exchanging sub-system were integrated into a power generation system. Valves and mass flow controllers in the sub-system were all electrically actuated versions, and the pump for coolant water delivery was electronically adjustable by external signals. A radiator and electrical fan were integrated into the heat exchanging sub-system, in which an electrical fan is optionally actuated in terms of a predetermined temperature of the coolant water.

In control unit, a programmable logic controller (PLC) was employed as the main control device, together with proper signal converters for optimization of signal orders to and from the devices in each sub-systems. Pre-built-in logics and equations in the PLC could control the gas feeding, cooling, and heat exchanging sub-systems. Pre-built-in equations for fuel and oxidant gas feed were established in a previous study of 1 kW class stack operation. The gas control scheme with these equations enables the system to conform to the external load change without being over-fed or fuel-starved in the cell stack (Fig. 16). The improved cell voltage distribution without end-cell voltage was achieved by means of this control scheme. The water pump was also

programmed to feed coolant water via PID control on the basis of the temperature control scheme and logic shown in Fig. 17, which was obtained in an earlier study with short stacks. This approach gave optimization of cell stack temperature.

All the operation and electrical performance-related parameters could be set-up and monitored in a touch screen device which was installed on the upper front part of the system (see Fig. 18). The operation logics and display screen configuration could be modified easily by connection

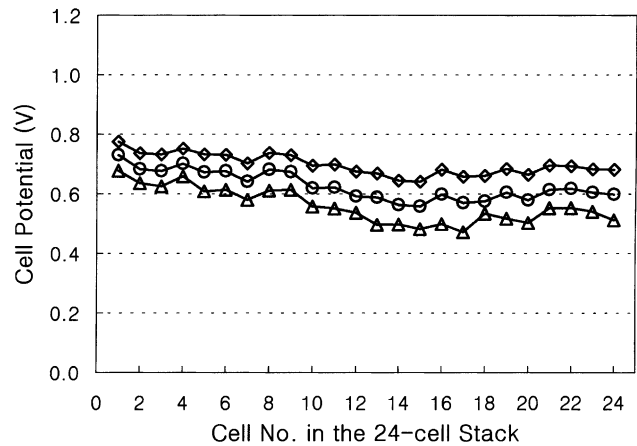


Fig. 16. Improved cell voltage distribution over 24-cell stack with optimized fuel-feed control scheme: (◇) 5 A; (○) 10 A; (△) 20 A.

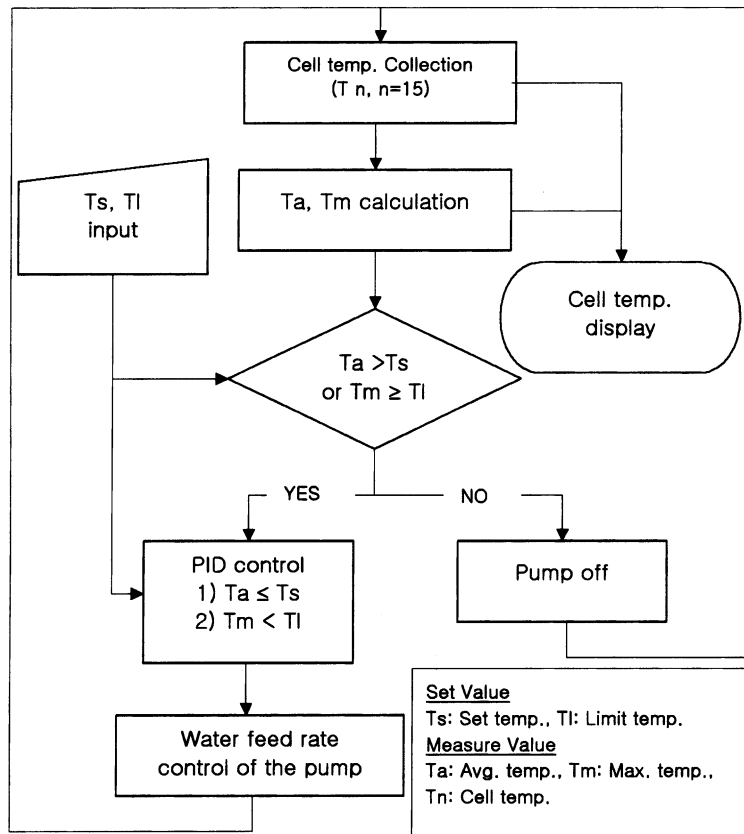


Fig. 17. Flow chart for thermal control logic.

of lap-top computer with on RS-232C cable. All operation data could also be acquired by the same lap-top computer with a commercial data acquisition program (Intouch™) and an additional communication module in the PLC unit. The touch screen consisted of eight screens, each screen

could be switched to another in random mode by touching the corresponding menu in the tool bar located in upper part of each screen. The functions of each touch screen are summarized in Table 3. The dc electric power produced in the system could be properly conditioned to ready-to-use

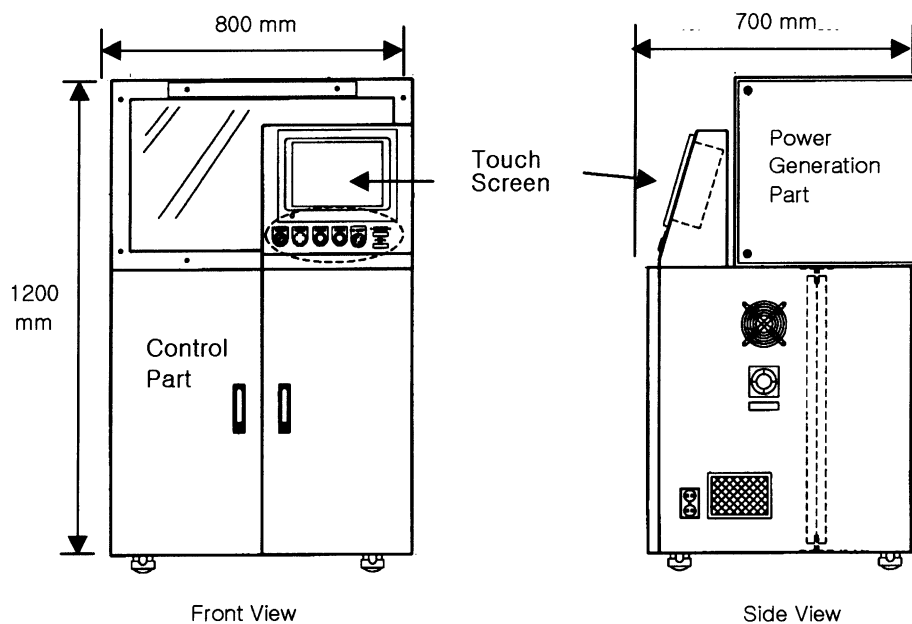


Fig. 18. Diagram of 1 kW class power generation system (exterior view).

Table 3
Summary of touch screen functions

Screen 1 (initial screen)	Screen 2 (start-up)	Screen 3 (set-up)	Screen 4 (stack data input)	Screen 5 (monitoring)	Screen 6 (temperature detail)	Screen 7 (coolant detail)	Screen 8 (output data)
Initialized screen	Solenoid valves for fuel and oxidant gas: on/off	Fuel/oxidant feed rate	Stack weight	Cell stack voltage	Maximum cell temperature	Water reservoir temperature	Output/unit weight
	Mass flow controllers for fuel and oxidant gas: on/off	Upper-limit temperature	Stack volume	External current load	Average stack temperature	Coolant feed rate set-up/display	Output/unit volume
	Coolant water pump: on/off	Optimum temperature	Cell number	Total electric output	Temperature set-up		Output/unit cell
	System error monitoring window	Gas feed control mode: manual/auto	Active electrode area	Maximum cell temperature	Each cell temperature monitoring		Output/unit area
				Average stack temperature	Temperature control mode: manual/auto		
				Fuel and oxidant gas feed rate			

220 VAC with a coupled dc/ac inverter, or could be consumed by the dummy load unit installed in the inverter.

3. Conclusions

1. A PEM fuel cell has effective proton conductivity only when its solid membrane is in a wet condition. A proton cannot migrate individually through the solid state membrane without water molecules. Thus, humidification of the fed gas is essential. The humidification process, however, can cause flooding of the electrode structure, which results in irreparable corrosion damage of the cell material. In this regard, proper thermal and fuel-feed control coordinated with water supply during extended operation time are critical to maintain the required wet and fuel-feed conditions in the cell structure to give reliability and longevity.
2. A 1 kW PEM fuel cell stack, a reactant gas feed sub-system, a heat exchanging sub-system and cooling sub-system with the PLC-based main control system were integrated into a 800 mm × 700 mm × 1200 mm single unit.
3. Experience with small-scale PEM fuel cell power generation systems can contribute to meeting the pending demand for large-scale systems. On going efforts based on the out comes of this study should be directed to the realization of power modules for large marine vessels, submarines and distributed industrial power plants.

Acknowledgements

The authors thank the General Director, Ik-Do Hur of Hyundai Industrial Research Institute (HIRI) for support and encouragement during this project. They are also grateful to other research staff at HIRI as well as Professor Jun-Bom Kim and his research team of University of Ulsan for their technical support and academic advice.

References

- [1] C. Sattler, J. Power Sources 71 (1998) 144–149.
- [2] H.I. Lee, T.Y. Oh, K.K. Baek, HIRI, HHI, Rep. No. AAD-HI3-1997, 217.
- [3] H.I. Lee, T.Y. Oh, K.K. Baek, HIRI, HHI, Rep. No. AAD-HI3-1998, 236.
- [4] H.I. Lee, T.Y. Oh, S.G. Choi, I.W. Park, K.K. Baek, HIRI, HHI, Rep. No. AAD-HI3-1999, 231.
- [5] C. Zawodzinski, M.S. Wilson, S. Gottesfeld, in: Proceedings of the 1st International Symposium on Proton Conducting Membrane Fuel Cells I, The Electrochemical Society Inc., 1995, pp. 57–65.
- [6] M. Mizuhata, K. Yasuda, K. Oguro, H. Takenaka, in: Proceedings of the 2nd International Fuel Cell Conference, NEDO, 1996, pp. 35–354.
- [7] S. Mukerjee, S. Srinivasan, M.P. Soriaga, J. Electrochem. Soc. 142 (5) (1995) 1409–1422.
- [8] E.J. Taylor, E.B. Anderson, N.R.K. Vilambi, J. Electrochem. Soc. 139 (5) (1992) 45–46.
- [9] M.S. Wilson, S. Gottesfeld, J. Electrochem. Soc. 139 (2) (1992) 28–30.
- [10] K. Mitsuda, T. Murahashi, J. Appl. Electrochem. 21 (1991) 524–530.